RSC Advances

ROYAL SOCIETY OF CHEMISTRY

www.rsc.org/advances

RSC Advances

PAPER

Methanol oxidation on Ru(0001) for direct methanol fuel cells: Analysis of the competitive reaction mechanism†

Xiaoqing Lu,[a*] Weili Wang,[a] Zhigang Deng,[b] Houyu Zhu,[a*] Shuxian Wei,[a] Siu-Pang Ng,[b] Wenyue Guo,[a*] Chi-Man Lawrence Wu[b]

The competitive oxidation reaction mechanism of methanol on Ru(0001) surface has been investigated by periodic density functional theory (DFT). Stable adsorption configurations, elementary reaction energies and barriers, the potential energy surface (PES), and the electrochemical potential analysis were elucidated. Results showed that O–H bond activation was more competitive than C–H and C–O bond activation during the initial methanol oxidation. Competitive pathways occurred for CH_3OH oxidation to CH_2O via $CH_3OH \rightarrow CH_3O \rightarrow CH_2O$ versus $CH_3OH \rightarrow CH_2OH \rightarrow CH_2O$, further to COOH via the CO pathway $CH_2O \rightarrow CHO \rightarrow CO \rightarrow COOH$ versus the non-CO pathway $CH_2O \rightarrow CH_2OOH \rightarrow CHOOH \rightarrow COOH$, and finally oxidation to CO_2. Taking PES and electrochemical potential analysis into account, $CH_3OH \rightarrow CH_2OH \rightarrow CH_2O \rightarrow CH_2OOH \rightarrow CHOOH \rightarrow COOH \rightarrow CO_2$ appeared to be the preferred oxidation pathway. The OH group could inhibit CO formation by directly reacting with CH_2O to yield CH_2OOH but could not efficiently remove CO that had already been produced by the reactions.

Received 00th xxxx 2015,
Accepted 00th xxxx 2015

DOI: 10.1039/x0xx00000x

www.rsc.org/advances

1. Introduction

Direct methanol fuel cells (DMFCs) have attracted widespread attention as clean, portable, and high-efficiency energy conversion devices that utilize the methanol (CH_3OH) oxidation reactions on catalysts. A large number of investigations have been performed to explore the catalysis mechanisms of CH_3OH on various pure metals, such as Ni,[1,2] Cu,[3, 4] Ag,[5] Pd,[6-10] Pt,[11-13] Rh,[14,15] and Ru.[16-19] Among these metals, Ru is generally applied as one of the main components of commercial catalysts in DMFC anodes, which can alleviate the problem of poor anode durability due to CO poisoning.[20-24] To achieve rational modification on the anode catalysts, many efforts have been devoted to understanding the CH_3OH oxidation mechanism on Ru catalyst experimentally. Unfortunately, although these studies were performed by using the same infrared absorption spectroscopy, conflicting evidence on adsorption and the reaction mechanism of CH_3OH oxidation have been observed on clean[16,17] and O-precovered[25,26] Ru(0001) surfaces. For the adsorption of reaction intermediates, Barros et al.[17] found upright and tilted methoxy (CH_3O) and formaldehyde (CH_2O); while Gazdzicki et al.[19] proposed an upright configuration of CH_3O. For CH_3OH oxidation, Gazdzicki et al.[18,19] found that CH_3OH was adsorbed as an intact molecule on clean and O-precovered Ru(0001) at temperatures below 80 K, while CH_3O was detected when annealing to 200-220 K; however, Barros et al.[27] observed spontaneous O–H bond breakage to form CH_3O for CH_3OH at 80 K. Although these contradictions exist, researchers generally agreed that CH_3OH could easily dehydrogenate on clean Ru(0001), leaving CO on its surface.[16,17]

From the theoretical point of view, CH_3OH oxidation on several clean metal surfaces has been investigated.[2,8,10-12,28-33] On Ni(111),[2] the favorable pathway of CH_3OH decomposition involved initial O–H bond scission, followed by sequential hydrogen abstractions to achieve the final products CO and H via CH_2O and CHO. On Pt(111),[11,12] the C–H bond scission of CH_3OH was the primary reaction process relative to the O–H bond scission, and the route $CH_3OH \rightarrow CH_2OH \rightarrow CHOH \rightarrow CO$ was suggested as the competitive pathway. On Pd(111), Schennach et al.[8] and Jiang et al.[10] found that initial C–H bond scission is preferable to that on Pt(111); by contrast, Zhang et al.[6] compared initial O–H and C–O bond scissions processes and found that O–H bond scission was energetically favorable. Despite difference in the bond scission mechanisms involved, production CO on clean metal surfaces appeared to be unavoidable. When considering the electrochemical environment induced by introduction of the OH group, theoretical calculations showed that CO poisoning could be alleviated by further oxidizing to CO_2 via $CO + OH \rightarrow COOH \rightarrow CO_2 + H$, which is regarded as "the CO pathway",[28-30] and/or by "the non-CO pathway" along $CHO + OH \rightarrow CHOOH \rightarrow CO_2 + 2H$.[31-33] Although Ru has been widely used in commercial DMFC anodes, the CH_3OH oxidation mechanism on Ru surfaces remains unclear because of contradictions observed in previous experiments and the lack of

[a] College of Science, China University of Petroleum, Qingdao, Shandong 266580, P. R. China.
[b] Department of Physics and Materials Science, City University of Hong Kong, Hong Kong SAR, P. R. China
E-mail: luxq@upc.edu.cn and wyguo@upc.edu.cn; Fax: +86-532-86983363; Tel: +86-532-86983372.
†Electronic Supplementary Information (ESI) available: The metastable adsorption configurations, and other elementary reaction steps with relatively high energy barriers in CH_3OH oxidation routes are presented. See DOI:10.1039/x0xx00000x

theoretical studies. Therefore, more details, including the most stable adsorption configuration, competitive reaction activation process, reaction thermodynamics and kinetics, and selectivity of production, are required to achieve a better understanding of CH_3OH oxidation on Ru catalyst.

In this work, the competitive oxidation reaction mechanism of methanol on Ru(0001) surface was investigated by using periodic density functional theory (DFT). The Ru(0001) surface is selected because it is thermodynamically stable and commonly used as a model system.[17,18] All possible adsorption structures and energies, elementary reaction steps, potential energy surface, and electrochemical potential analysis were elucidated along the competitive pathways from CH_3OH to CH_2OH, COOH, and CO_2. The findings of this study are expected to provide deeper insights into the catalytic performance of Ru, adsorption selectivity, sequence of bond scission, competition of elementary reaction processes, thermodynamic and kinetic properties, and thus highlight the intrinsic characteristics of methanol oxidation on Ru(0001) in DMFCs.

2. Computational methods

All calculations were performed in the DFT framework with DMol^3 in Materials Studio (Accelrys Inc.).[34] The exchange-correlation energy was calculated within the generalized gradient approximation (GGA) using Perdew and Wang (PW91) functional.[35,36] To take the relativity effect into account, the density functional semicore pseudopotential (DSPP)[37,38] method was employed for Ru atoms, and C, H and O atoms were treated with the all-electron basis set. The valence electron functions were expanded into a set of numerical atomic orbitals by a double-numerical basis with polarization functions (DNP). Fermi smearing of 0.005 Hartree and a real-space cutoff of 4.7 Å were used to improve the computational performance.[39,40] Transition state (TS) searches were performed at the same theoretical level by using the complete LST/QST method.[41] The convergence criterion for the TS searches was set to 0.272 eV/Å for the root-mean-square of atomic forces. Vibrational frequencies were calculated for all the initial states (ISs) and final states (FSs), as well as the TSs from the Hessian matrix with harmonic approximation. Zero-point energy (ZPE) was calculated from the resulting frequencies.[42]

Ru(0001) surface was modeled with a three-layer slab with nine Ru atoms per layer representing a (3 × 3) surface unit cell; a vacuum region of 12 Å thickness was used to separate the surface from its periodic image in the direction along the surface normal. The reciprocal space was sampled with a (4 × 4 × 2) *k*-point grid using the Monkhorst–Pack method.[43] A single adsorbate was allowed to adsorb on one side of the unit cell, corresponding to a surface coverage of 1/9 ML. Full-geometry optimization was performed for relevant adsorbates and the uppermost two layers without symmetry constraints, while the bottom layer Ru atoms were fixed to their bulk-truncated positions with the experimentally determined lattice parameters of $a = b = 2.71$ Å and $c = 4.28$ Å. Nonperiodical structures were fully optimized at the same theoretical level for the isolated atoms, radicals and molecules involved.

The adsorption energies reported herein are calculated using the equation:

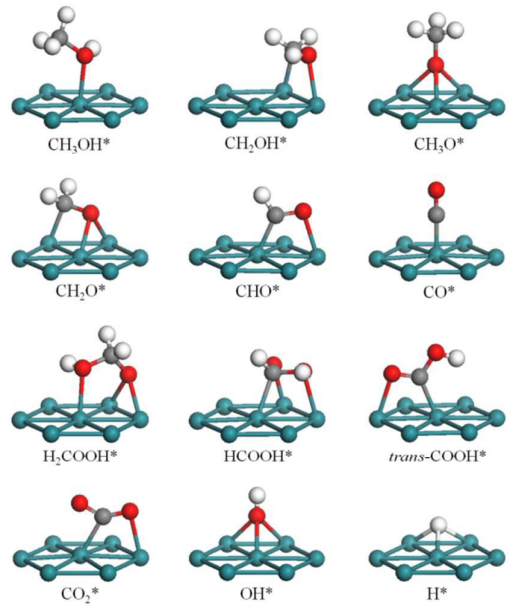

Fig. 1 The most stable adsorption configurations of intermediates involved in CH_3OH oxidation on Ru(0001). The C, O, H, and Ru atoms are shown in gray, red, white, and light-blue colors, respectively.

$$E_{ads} = E_{adsorbate} + E_M - E_{adsorbate/M} \quad (1)$$

where E_{ads} is the adsorption energy of the adsorbate on the metal surface; $E_{adsorbate}$, E_M and $E_{adsorbate/M}$ are the energies of the free adsorbate, the clean Ru(0001) slab, and the adsorbate/M adsorption system, respectively. By this definition, the stable adsorption will have a positive adsorption energy.

3. Results and discussion

For clarity, this section is organized as follows: First, adsorption structures and energies for most of the intermediates are presented. Then, the possible elementary reactions along with the relevant reaction network are elucidated. Next, the overall PES for competitive pathways is discussed. Finally, the CH_3OH electrooxidation process on Ru(0001) is analyzed. All energies reported herein are with ZPE corrections.

3.1 Adsorption

Table 1 tabulates the adsorption information for the most stable adsorption modes of intermediates involved, and the corresponding configurations are shown in Fig. 1. Structural parameters and geometries of other intermediates are presented in Table S1 and Fig. S1 (Electronic Supporting Information).

Methanol (CH_3OH). For gas-phase CH_3OH, the bond lengths are calculated to be 1.10 Å for the C–H bonds, 1.43 Å for the C–O bond, and 0.97 Å for the O–H bond, in good agreement with the experimental values of 1.09, 1.43, and 0.95 Å, respectively.[44] CH_3OH can be stabilized on Ru(0001) without spontaneous decomposition, thus confirming the experimental observation.[18,19] CH_3OH prefers the adsorption at top site of Ru(0001) through

Table 1. Adsorption sites, adsorption energies (in eV), and structural parameters (in angstroms and degrees) for intermediates involved in CH_3OH oxidation on Ru(0001).

species	site	mode	E_{ads}	$d_{C/H-Ru}$	d_{O-Ru}	angles[a]
CH_3OH^*	top	η^1(O)	0.56		2.31	53
CH_2OH^*	bridge	η^1(C)-η^1(O)	1.98	2.14	2.28	90
CH_3O^*	fcc	η^3(O)	2.52		2.20, 2.20, 2.20	0
	hcp	η^3(O)	2.54		2.19, 2.19, 2.19	0
CH_2O^*	top	η^1(O)	0.45		2.20	49
	fcc	η^1(C)-η^2(O)	0.90	2.15	2.20, 2.20	79
	hcp	η^1(C)-η^2(O)	0.96	2.15	2.18, 2.18	79
CHO^*	bridge	η^1(C)-η^1(O)	2.44	1.99	2.19	81
	fcc	η^2(C)-η^1(O)	2.26	2.12	2.15, 2.19	76
	hcp	η^2(C)-η^1(O)	2.36	2.11	2.13, 2.17	76
CO^*	top	η^1(C)	1.93	1.89		0
	bridge	η^2(C)	1.66	2.08, 2.08		0
	fcc	η^3(C)	1.70	2.15, 2.16, 2.17		0
	hcp	η^3(C)	1.71	2.14, 2.14, 2.15		0
CH_2OOH^*	fcc	η^1(O)-η^2(O)	2.73		2.24, 2.22, 2.22	42, 67
	hcp	η^1(O)-η^2(O)	2.77		2.32, 2.19, 2.21	43, 72
$CHOOH^*$	fcc	η^1(C)-η^2(O)	0.62	2.19	2.10, 2.28	87, 90
	hcp	η^1(C)-η^2(O)	0.66	2.18	2.09, 2.27	88, 90
trans-$COOH^*$	bridge	η^1(C)-η^1(O)	2.69	2.05	2.20	33, 83
cis-$COOH^*$	bridge	η^1(C)-η^1(O)	2.68	2.05	2.21	31, 85
CO_2^*	bridge	η^1(C)-η^1(O)	0.05	2.10	2.22	59, 79
OH^*	top	η^1(O)	2.84		1.99	
	bridge	η^2(O)	3.14		2.16, 2.16	
	fcc	η^3(O)	3.19		2.21, 2.21, 2.21	
	hcp	η^3(O)	3.19		2.20, 2.20, 2.20	
H^*	bridge	η^2(H)	2.80	1.82, 1.82		
	fcc	η^3(H)	2.91	1.90, 1.91, 1.92		
	hcp	η^3(H)	2.87	1.90, 1.91, 1.92		

[a] Values are angles between the surface normal and the C-O axis in the corresponding species.

oxygen via donation of the lone pair to metallic surfaces[45,46] with the O–Ru distance of 2.31 Å, as shown in Fig. 1 and Table 1. The C–O axis tilts by 53° relative to the surface normal, thereby facilitating binding of CH_3OH to the surface via the oxygen lone pair orbital.[47] The adsorption energy is calculated to be 0.56 eV; this relatively weak adsorption is consistent with the large O–Ru distance as well as the small structural deformation of CH_3OH upon adsorption. Similar adsorption configurations of CH_3OH can be found on Ni(111),[2] Pt(111),[12] and Pd(111).[10]

Hydroxymethyl (CH_2OH). CH_2OH is obtained from CH_3OH dehydrogenation via C–H bond scission, and tends to adsorb at bridge site through the η^1(C)-η^1(O) mode. The C–O axis is almost parallel to the surface, and the C–Ru and O–Ru distances are 2.14 and 2.28 Å, respectively. The adsorption energy is calculated to be 1.98 eV. Different from that on Ru(0001), CH_2OH on Ni(111),[2] Pt(111),[12] and Pd(111)[10] prefers to adsorb at top site of the metal atom through the C atom.

Methoxy (CH_3O). The initial O–H bond breaking of CH_3OH produces CH_3O. CH_3O prefers to bind at hollow (hcp) site in an upright configuration, as shown in Fig. 1. This finding agrees well with the IR spectral observation that CH_3O is adsorbed in a C_{3v} symmetry with the C–O axis parallel to the surface normal.[17] The O–Ru bond length is calculated to be 2.19 Å, in good agreement with Gazdzicki's experimental result of 2.19 Å.[19] The binding energy is 2.54 eV, as shown in Table 1. These results agree well with the previous DFT study of CH_3O adsorption on Ru cluster,[48] wherein CH_3O was observed to locate at hollow site in an upright configuration with a binding energy of 2.39 eV.

Formaldehyde (CH_2O). CH_2O is an important intermediate in CH_3OH decomposition and synthesis.[49] Our calculations show that CH_2O tends to anchor on the Ru(0001) surface at hollow site via the η^1(C)–η^2(O) mode, as shown in Fig. 1. The C–Ru bond length is 2.15 Å, and the two O–Ru bond lengths are both 2.18 Å; the C–O axis is titled by 79° relative to the normal of the substrate (Table 1). The adsorption energy is calculated to be 0.96 eV. On Rh(111), the η^1(C)-η^2(O) mode of CH_2O is also the most stable structure with a binding energy of 0.98 eV.[15] On group VIII metal surfaces, CH_2O generally adsorbs via the η^1(C)–η^1(O) mode,[45] stabilizing the system by 0.45 - 0.63 eV on Pd(111),[8-10] 0.50 eV on Pt(111),[11, 12] and 1.03 eV on Ni(111).[2]

Formyl (CHO). The most stable configuration of CHO favors the η^1(C)-η^1(O) adsorption mode at bridge site. As shown in Fig. 1, CHO binds to the metal surface through C and O atoms anchored at two adjacent top sites; the C–Ru and O–Ru bond lengths are 1.99 and 2.19 Å, respectively. The adsorption energy is calculated to be 2.44 eV. On Pt(111)[11] and Pd(111),[10] CHO prefers to bind at hollow site with an η^2(C)-η^1(O) mode, where the C atom sits over a bridge site and the O atom on top of an adjacent Pd atom.

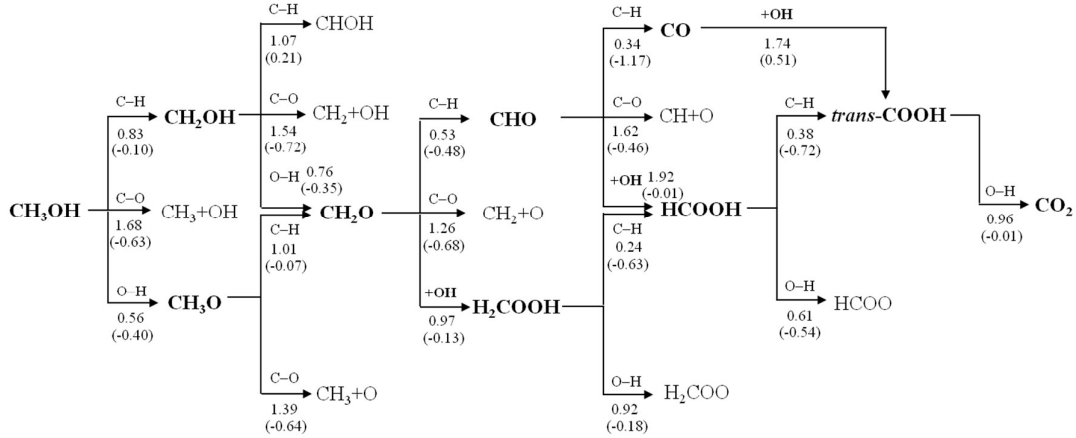

Fig. 2 The reaction network for CH_3OH oxidation on Ru(0001). "A–B" represents the "A–B" bond scission and "+OH" means the combination with OH group. The energy barrier and reaction energy (in parentheses) are in eV. For simplicity, the H atom is omitted.

CH_2OOH, Formic acid (CHOOH) and Carboxyl (COOH). CH_2OOH is generated by the association of CH_2O with OH, which prefers to adsorb at hcp site via two O atoms. One O atom binds at top site while the other at bridge site, and the CH_2 group is repelled away from the surface. The distances between O atoms and the surface Ru atoms are 2.32, 2.19 and 2.21 Å, respectively. The O–C–O angle is calculated to be 113°, and the adsorption energy is 2.77 eV. CHOOH binds at hcp site with the η^1(C)-η^2(O) mode. The C–H bond is located away from the surface whereas the O–H bond is parallel to the surface. The adsorption energy of CHOOH is calculated to be 0.66 eV. COOH is stabilized over bridge site via the η^1(C)-η^1(O) mode. Two opposite orientations of O–H bond lead to two stable isomers of COOH: *trans*-COOH (Fig. 1) and *cis*-COOH (Fig. S1) with the binding energies of 2.69 and 2.68 eV, respectively. The adsorption configuration of *trans*-COOH characterizes bond lengths of 2.20 and 2.05 Å for the O–Ru and C–Ru bonds, respectively.

Carbon monoxide (CO) and Carbon dioxide (CO_2). CO prefers to vertically occupy top site on the Ru(0001) surface via the C atom. The C–Ru bond length is 1.89 Å and the adsorption energy is 1.93 eV. CO tends to bind at hollow site on Pd(111)[10] and Pt(111)[13] with adsorption energies of about 1.80 and 1.74 eV, respectively. CO_2 locates at bridge site on Ru(0001) with an adsorption energy as low as 0.05 eV; such an energy indicates easy desorption of CO_2 from the surface. The C–Ru and O–Ru bond lengths are 2.10 and 2.22 Å, respectively.

Hydroxyl (OH) and Hydrogen (H). OH can stably locate at hollow site through the O atom with an upright configuration. OH has the same adsorption energy of 3.19 eV for both hcp and fcc sites. Koper et al.[13] studied OH binding on Ru(0001) using the DFT slab model and obtained adsorption energies of 3.52 and 3.49 eV for stable adsorption at fcc and hcp sites, respectively. Atomic H is energetically favored to adsorb at hollow site on the Ru(0001) surface, consistent with the results of a previous electron energy loss spectroscopy study.[50] The adsorption energy of atomic H is 2.91 eV, agreeing well with previous DFT study of H adsorption on a Ru surface (E_{ads} = 2.90 eV).[51]

3.2 Initial oxidation of CH_3OH to CH_2O

The reaction network of CH_3OH oxidation on Ru(0001) is shown in Fig. 2. Structures of IS, TS, and FS along elementary reaction steps are presented in Figs. 3-6. As a whole, CH_3OH dehydrogenates to CH_2O via the competitive routes of $CH_3OH \rightarrow CH_3O \rightarrow CH_2O$ and/or $CH_3OH \rightarrow CH_2OH \rightarrow CH_2O$ (Fig. 3), then further oxidizes to *trans*-COOH via the CO pathway $CH_2O \rightarrow CHO \rightarrow CO \rightarrow COOH$ (Fig. 4) and/or the non-CO pathway $CH_2O \rightarrow CH_2OOH \rightarrow CHOOH \rightarrow COOH$ (Fig. 5), and achieve CO_2 eventually (Fig. 6). For brevity, other elementary reaction steps with relatively high energy barriers are described in Fig. S2, including the C–O bond scissions of CH_3OH, CH_3O, CH_2OH, CH_2O, and CHO, the combination of CHO and OH to CHOOH, the reaction of CO with OH to *cis*-COOH, the dehydrogenation of CH_2OOH to CH_2OO, and further dehydrogenation to CHOO.

Three possible initial bond scissions of CH_3OH are considered, that is, O–H, C–H and C–O bond scissions. C–O bond scission involves a very high energy barrier of 1.68 eV, whereas O–H bond scission involves a relatively low energy barrier of 0.56 eV. The reaction $CH_3OH \rightarrow CH_3O + H$ leads to elongation of the O–H bond length to 2.10 Å in TS1 (Fig. 3a) relative to 0.98 Å in IS and yields coadsorbed CH_3O and H atom on adjacent hcp sites as FS. As shown in Fig. 3b, C–H bond scission is mirrored by an elongated C–H bond length of 1.58 Å in TS2, together with the CH_2OH group bending towards the surface and the H atom moving to adjacent bridge site. The energy barrier of $CH_3OH \rightarrow CH_2OH + H$ is 0.83 eV. The reaction process of $CH_3OH \rightarrow CH_3 + OH$ is presented in Fig. S2. The activation energies of the C–H and C–O bonds are higher than that of the O–H bond, indicating that initial O–H bond scission of CH_3OH is highly favorable on Ru(0001). During initial oxidation of CH_3OH, O–H bond scission is also preferable on Cu(111)[52] and Ag(111),[5] while C–H bond scission is more facile on Pd(111) and Pt(111).[53, 54]

Subsequently, C–H bond scission of CH_3O starts with its most stable configuration at hcp site and ends with CH_2O at hcp site and H atom at fcc site, as shown in Fig. 3c. In TS3, the C–O axis tilts towards the surface with the O atom above bridge site, thereby

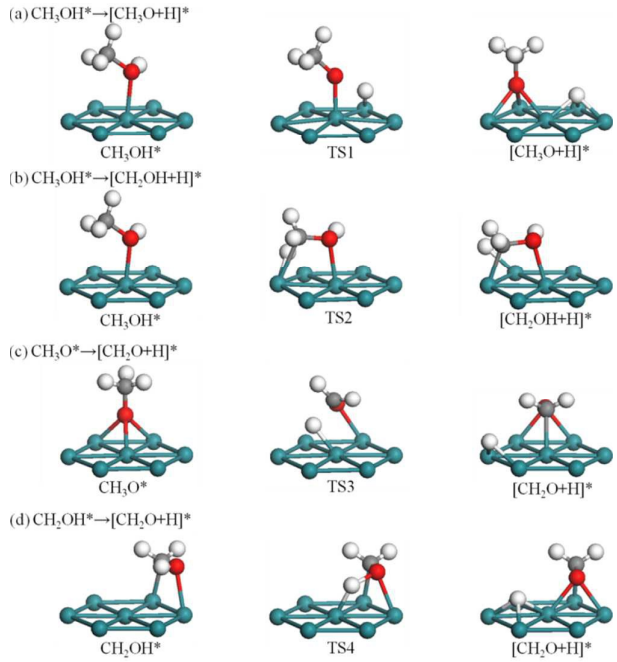

Fig. 3 Dehydrogenation of CH_3OH to CH_2O through $CH_3OH \rightarrow CH_3O \rightarrow CH_2O$ (a, c) and $CH_3OH \rightarrow CH_2OH \rightarrow CH_2O$ (b, d). [A + B]* denotes the coadsorbed A and B species.

facilitating the C–H bond scission. The energy barrier is calculated to be 1.01 eV and the reaction is exothermic by 0.07 eV. For CH_2OH, C–H bond scission involves a high energy barrier of 1.07 eV relative to the 0.76 eV of its O–H bond scission. As shown in Fig. 3d, O–H bond scission of CH_2OH yields CH_2O at fcc site and the H atom at hcp site. The O–H bond length is elongated to 1.48 Å in TS4, and a slight swag vibration facilitates removal of the H atom.

3.3 CH_2O oxidation to COOH via the CO pathway

As shown in Fig. 4a, dehydrogenation of CH_2O to CHO involves rotation of CH_2O along the C–O bond axis, so that one of the H atoms can easily approach a surface Ru atom and form a Ru–H bond. This process is exothermic by 0.48 eV and the energy barrier is 0.53 eV. By comparison, C–O bond scission requires a higher energy barrier of 1.26 eV, as shown in Fig. S2c and Table S1.

Fig. 4b illustrates that dehydrogenation of CHO starts with CHO binding at bridge site in IS and ends with CO sitting atop a Ru atom in FS. In TS5, CHO is located at off-top site and the C–H bond is elongated by 0.10 Å; C–H bond scission is triggered by a swag vibration of the adsorbed CHO, giving rise to the H atom close to the surface. This process is strongly exothermic by 1.17 eV with a relatively low energy barrier of 0.34 eV. Comparatively, C–O bond scission and combination of CHO with OH to form CHOOH involve energy barriers of up to 1.62 and 1.92 eV, respectively, as shown in Figs. S2c and S2d and Table S1.

Oxidation of the adsorbed CO by OH can produce *trans*-COOH and *cis*-COOH in FS. The energy barriers for these reaction steps are as high as 1.74 and 2.07 eV, respectively. To achieve the formation of *trans*-COOH, as shown in Fig. 4c, CO and OH groups approach each other together with the elevation of the OH group in TS6.

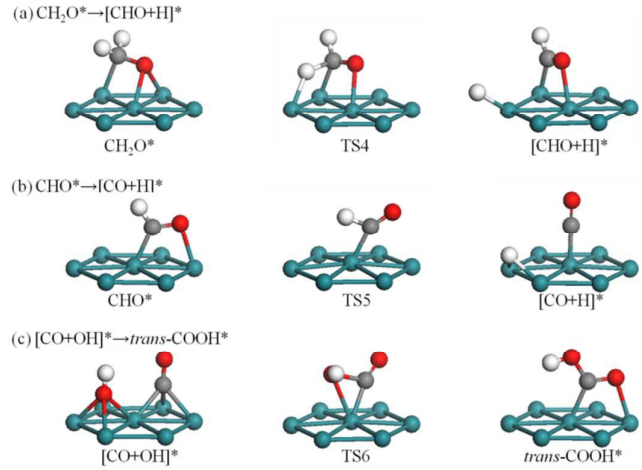

Fig. 4 The CO pathway for CH_2O oxidation to *trans*-COOH.

3.4 CH_2O oxidation to COOH via the non-CO pathway

CH_2O can react with OH to form CH_2OOH on Pd,[53] Ag,[54,55] and Cu.[56] In the real electrochemical environment of DMFCs, the OH group usually comes from the reaction between coadsorbed H_2O and O_{ad} ($H_2O + O_{ad} \rightarrow 2OH$)[57] or direct decomposition of H_2O ($H_2O \rightarrow H + OH$). On Ru(0001), the adsorbed CH_2O at hcp site reacts with OH at fcc site in IS and ends with CH_2OOH at hcp site, as shown in Fig. 5a. The binding energy for coadsorbed CH_2O and OH is 5.68 eV, much higher than the sum of their individual adsorption energies of 0.96 eV for CH_2O and 3.19 eV for OH. This result indicates the strong attraction between CH_2O and OH, which stabilizes the coadsorption system so as to further bind these two species. In TS7, the OH group migrates to bridge site, thus facilitating interactions with the elevated CH_2 group in CH_2O. The energy barrier here is 0.97 eV, and the reaction is exothermic by 0.13 eV.

As shown in Fig. 5b, CH_2OOH dehydrogenation via C–H bond scission results in CHOOH located at top site and the H atom at hcp site. In TS8, the C–H bond is broken and the detached H atom sits at top site. This process is exothermic by 0.63 eV, and the energy barrier is 0.24 eV. CH_2OOH dehydrogenation can also proceed via O–H bond scission (Fig. S2g), that is, $CH_2OOH \rightarrow CH_2OO + H$. The barrier here is 0.92 eV and the reaction energy is 0.18 eV.

Fig. 5c illustrates C–H bond scission of CHOOH, which starts with CHOOH located at hcp site and ends with *trans*-COOH at bridge site and H atom at fcc site. In TS9, the C–H bond distance is elongated by 0.21 Å with the OH group detached from the surface; slight rotation of the C–O bond facilitates the C–H bond scission. This dehydrogenation step is exothermic by 0.72 eV, and the energy barrier is 0.38 eV. O–H bond scission for CHOOH (CHOOH → CHOO + H, Fig. S2h) involves an energy barrier of 0.61 eV and a reaction energy of 0.54 eV.

3.5. Formation of CO_2

Fig. 6 reveals that stretch vibrations of the O–H bond can induce the H atom of *trans*-COOH to approach the surface such that *trans*-COOH decomposes to COO and atomic H. Obviously, O–H bond scission is more likely to take advantage of the downward-facing mode of *trans*-COOH than the up-facing mode of *cis*-COOH. In

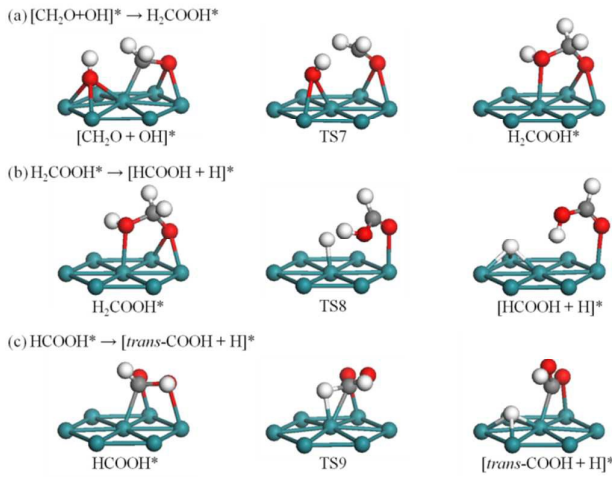

Fig. 5 The non-CO pathway for CH_2O oxidation to *trans*-COOH.

TS10, the CO_2 fragment remains at bridge site while the O–H bond is broken with an O–H distance of 1.53 Å. This process is almost thermoneutral with a reaction energy of 0.01 eV and an energy barrier of 0.96 eV.

3.6. Potential energy surface (PES)

The overall PES of CH_3OH oxidation on Ru(0001) is illustrated in Fig. 7, including three-stage oxidation products of CH_2O, COOH and CO_2. Competitive pathways appear for the first two steps, that is, $CH_3OH \rightarrow CH_3O \rightarrow CH_2O$ versus $CH_3OH \rightarrow CH_2OH \rightarrow CH_2O$ for CH_2O; and the CO pathway $CH_2O \rightarrow CHO \rightarrow CO \rightarrow$ *trans*-COOH versus the non-CO pathway $CH_2O \rightarrow CH_2OOH \rightarrow CHOOH \rightarrow$ *trans*-COOH for COOH.

For CH_3OH oxidation to CH_2O, the dehydrogenation sequence plays a crucial role in the reaction kinetics via two competitive pathways. Along the $CH_3OH \rightarrow CH_3O \rightarrow CH_2O$ pathway, the activation energies of O–H and C–H bond scission are 0.56 and 1.01 eV, respectively. By comparison, along the $CH_3OH \rightarrow CH_2OH \rightarrow CH_2O$ pathway, the energy barriers of C–H and O–H bond scissions are 0.83 and 0.76 eV, respectively. Thus, to achieve oxidation of CH_3OH on Ru(0001), initial O–H bond scission (E_a = 0.56 eV) is more facile than the C–H bond scission (E_a = 0.83 eV). Once CH_3O is formed, subsequent C–H bond scission involves a larger barrier of 1.01 eV. Therefore, CH_3O can accumulate to a certain extent on the Ru surface, which explains why CH_3O is consistently detected in the experiments.[18, 19] Considering the relative smooth PES, the $CH_3OH \rightarrow CH_2OH \rightarrow CH_2O$ pathway is more competitive for forming CH_2O than the $CH_3OH \rightarrow CH_3O \rightarrow CH_2O$ pathway.

For CH_2O oxidation to COOH, the energy barriers along the CO pathway are 0.53 eV for $CH_2O \rightarrow CHO$, 0.34 eV for $CHO \rightarrow CO$, and 1.74 eV for $CO + OH \rightarrow COOH$. The rate-determining step along the CO pathway appears to be the combination of CO and co-adsorbed OH to form COOH. By comparison, the energy barriers along the non-CO pathway are 0.97 eV for $CH_2O + OH \rightarrow CH_2OOH$, 0.24 eV for $CH_2OOH \rightarrow CHOOH + H$, and 0.38 eV for $CHOOH \rightarrow COOH + H$. The rate-determining step along the non-CO pathway

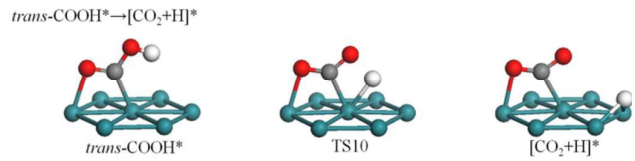

Fig. 6 Formation of CO_2 via dehydrogenation of *trans*-COOH.

appears to be the combination of CH_2O and co-adsorbed OH to produce CH_2OOH. Note that the rate-determining steps along both pathways appear when reacting with the coadsorbed OH to form the C–O bond. Comparing these two pathways, CO seems to be easier to form along the CO pathway and accumulate on Ru(0001) because of the high energy barrier required for further combination with OH. However, since the OH group pre-exists in the electrolyte and has a much larger adsorption energy than CO (2.84 - 3.19 eV for OH versus 1.66 - 1.93 eV for CO, Table 1), most of the adsorption sites would be covered by OH under working conditions. Thus, the coverage of newly-formed CO is low and the formation of CO on Ru(0001) is inhibited. Comparatively, the non-CO pathway is more favorable and followed by COOH dehydrogenization to form CO_2. Participation of the OH group on Ru(0001) avoid the CO formation during CH_3OH oxidation along the non-CO pathway, but cannot remove the CO that had already been produced because of the very high barriers involved in the transformation of $CO + OH \rightarrow COOH$ (1.74 eV for *trans*-COOH and 2.07 eV for *cis*-COOH).

3.7. Electrochemical potential analysis

The standard hydrogen electrode (SHE)[58] is used to treat the electrochemical potential (U). The overall electrochemical reaction on the anode of a DMFC is: $CH_3OH + H_2O \rightarrow CO_2 + 6H^+ + 6e^-$. Under standard conditions, the free energy of two protons and two electrons at zero potential is equal to the free energy of a hydrogen molecule. The change in free energy at a given potential U of a reaction involving the formation of a proton electron pair versus that at the SHE is equivalent to $\Delta G = -eU$, where e is the charge on the electron. Additionally, intermediates that are closed-shell molecules (e.g., CH_3OH and CO_2) are treated as gas-phase molecules, as the bond energy to the surface will be unlikely to overcome the entropy loss through surface binding. Based on this approach, the required lowest potential U can be obtained to discuss the competitive reaction pathways of CH_3OH electro-oxidation on Ru(0001), as successfully applied in similar reactions.[54,58-60] The details of this method refer to the previous literature.[54,59]

The free energies of all of the intermediates are calculated relative to $H_2O(l)$, $CO_2(g)$ and $H_2(g)$, as presented in Table 2. The free energy of CH_3OH, for example, is calculated as follows,

$$CO_2(g) + 3H_2(g) \rightarrow CH_3OH(g) + H_2O(l) \quad (2)$$

$\Delta G_{CH_3OH} = TE_{H_2O} + TE_{CH_3OH} - TE_{CO_2} - 3*TE_{H_2} + ZPE_{H_2O} + ZPE_{CH_3OH} - ZPE_{CO_2} - 3\times ZPE_{H_2} - T\times(S_{H_2O} + S_{CH_3OH} - 3\times S_{H_2} - S_{CO_2})$, where TE is the total energy of the reactant and product species, T is the standard temperature (298 K), ZPE is the zero-point energy, and S is the entropy of the species. For gas- and liquid-phase molecules, the entropy values are taken from the literature.[61]The free energies of surface intermediates are also calculated in a similar manner,

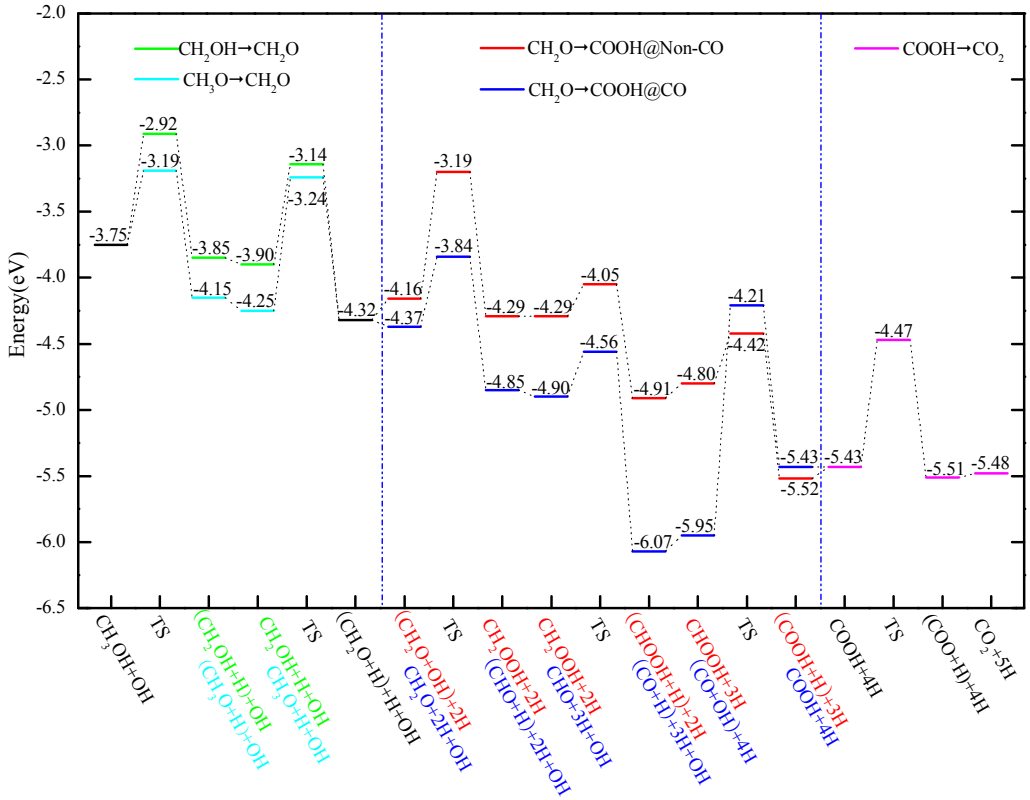

Fig. 7 PES of CH_3OH oxidation on Ru(0001). All energies (eV) are relative to the energy gaseous molecules of hydroxy and one gaseous molecule of methanol plus the clean Ru(0001) surface with ZPE corrections. [A+B]* denotes the coadsorbed A and B, and A*+ B* represents respective adsorptions of A and B on two separated slabs.

Table 2. Calculated free energies ΔG (in eV) of adsorbed intermediates and closed-shell gas-phase intermediates at standard conditions (298 K, 1 bar) for CH_3OH electrooxidation on Ru(0001).[a]

CH_3OH	CH_3O	CH_2OH	CH_2O	H_2COOH	CHO	CHOOH	CO	COOH	CO_2
0.10	-0.01	0.32	0.63	0.36	0.16	0.28	-0.79	-0.05	0.00

[a] CO_2(g), H_2O(l), and H_2(g) are used as reference. Zero-point energy and entropy corrections are included.

for example,

$$CO_2(g) + 2.5H_2(g) + * \rightarrow CH_3O^* + H_2O(l) \quad (3)$$

$\Delta G_{CH_3O^*} = TE_{H_2O} + TE_{CH_3O^*} - TE_{CO_2} - 2*TE_{H_2} - TE_{clean} + ZPE_{H_2O} + ZPE_{CH_3O^*} - ZPE_{CO_2} - 2.5*ZPE_{H_2} - T*(S_{H_2O} + S_{CH_3O^*} - 2.5*S_{H_2} - S_{CO_2})$, where TE_{clean} is the total energy of the clean slab, $TE_{CH_3O^*}$ is the total energy of CH_3O^* adsorbed on a clean slab, and $ZPE_{CH_3O^*}$ and $S_{CH_3O^*}$ are the zero-point energy and entropy for the adsorbed CH_3O^*, respectively. For molecules bound to the surface, the vibrational entropy is calculated assuming a quantum mechanical harmonic oscillator with the same vibrational frequencies as those applied to the zero-point energy. As shown in Table 2, the free energies for closed-shell gas-phase intermediates are as follows: CH_3OH = 0.10 eV, CH_2O = 0.63 eV, CHOOH = 0.28 eV, and CO_2 = 0.0 eV; these values are comparable with previous DFT results[54] of 0.11, 0.71 eV, 0.42 eV, and 0.0 eV, respectively. As a reference, the standard table values are: CH_3OH(g) = 0.05 eV, CH_2O(g) = 0.57 eV, CHOOH(g) = 0.44 eV, and CO(g) = 0.0 eV. The negative values of adsorbed CH_3O, CO, and COOH indicate that these surface intermediates are thermodynamically more stable than the reference molecules at standard conditions [i.e., CO_2(g), H_2O(l), and H_2(g) at 298 K and 1 bar pressure]. Of these intermediates, CO has the lowest free energy because of its strong bonding with Ru(0001), as noted previously. Positive values of all other adsorbed intermediates (i.e., CH_2OH, CH_2OOH, and CHO) suggest that the surface species is not as stable as the reference molecules at standard conditions; thus, the reaction to form the reference molecules from the surface species would be exothermic on Ru(0001) at standard conditions.

A comparison of the electrochemical potentials for the competitive reactions on Ru(0001) is shown in Fig. 8. For the initial CH_3OH oxidation processes $CH_3OH \rightarrow CH_3O$ versus $CH_3OH \rightarrow CH_2OH$, a lower potential is required to strip off the hydroxyl proton than that required to strip off the methoxyl proton, in agreement with previous experimental observations.[62] Similar case takes place for proton stripped from the hydroxyl with a lower potential along the

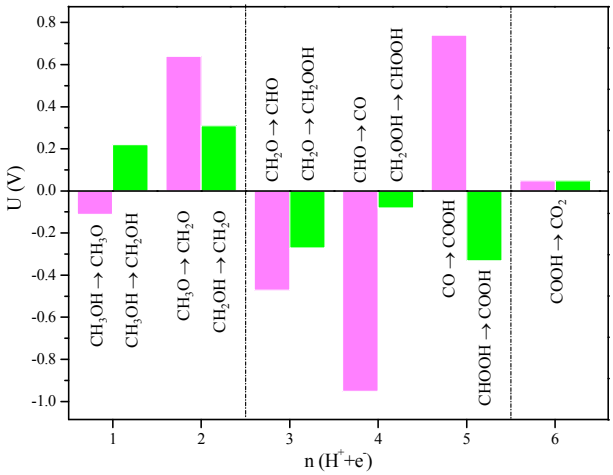

Fig. 8 The electrochemical potentials for CH_3OH oxidation on Ru(0001). The x-axis indicates how many proton/electron pairs have been created from CH_3OH.

subsequent oxidation to formaldehyde ($CH_2OH \rightarrow CH_2O$ versus $CH_3O \rightarrow CH_2O$). Along the CO pathway $CH_2O \rightarrow CHO \rightarrow CO \rightarrow COOH$, the highest potential is calculated to be 0.74 V for CO + OH → COOH; by contrast, the non-CO pathway $CH_2O \rightarrow CH_2OOH \rightarrow CHOOH \rightarrow COOH$ requires a much lower potential than 0.74 V. Therefore, at low potentials, CH_3OH electrooxidation on Ru(0001) proceeds primarily via the non-CO pathway to produce CO_2; at high potentials, both the CO and non-CO pathways are thermodynamically available on Ru(0001).

4. Conclusions

Our theoretical investigation provides a systematic understanding of the competitive oxidation reaction mechanism of methanol on Ru(0001) surface for DMFCs. The following findings are obtained:

(1) To achieve a stable adsorption configuration, CH_3OH and CO prefer to adsorb at top site, CH_2OH, CHO and COOH prefer to adsorb at bridge site, and CH_3O, CH_2O, CH_2OOH and CHOOH prefer to adsorb at hollow site on the Ru(0001) surface.

(2) O–H bond activation is more competitive than C–H and C–O bonds activations during CH_3OH and CH_2OH oxidation. Competitive oxidation pathways to CH_2O occur via $CH_3OH \rightarrow CH_3O \rightarrow CH_2O$ versus $CH_3OH \rightarrow CH_2OH \rightarrow CH_2O$, further to COOH by virtue of OH group via the CO pathway $CH_2O \rightarrow CHO \rightarrow CO + OH \rightarrow COOH$ versus the non-CO pathway $CH_2O + OH \rightarrow CH_2OOH \rightarrow CHOOH \rightarrow COOH$, and finally oxidation to CO_2. For both the CO and non-CO pathways, the rate-determining step appears to be the C–O bond formation when interacting with the OH group.

(3) PES analysis confirms that $CH_3OH \rightarrow CH_2OH \rightarrow CH_2O \rightarrow CH_2OOH \rightarrow CHOOH \rightarrow COOH \rightarrow CO_2$ is the preferred pathway, agreeing well with the electrochemical potential analysis for CH_3OH electro-oxidation. The OH group could inhibit CO formation by directly reacting with CH_2O to yield CH_2OOH, but cannot remove the CO that had already been produced.

Acknowledgements

This work was supported by NSFC (21303266), National Basic Research Program of China (2014CB239204), Promotive Research Fund for Excellent Young and Middle-aged Scientists of Shandong Province (BS2013CL031), and the Fundamental Research Funds for the Central Universities (15CX05050A, 15CX08010A, 14CX02214A).

Notes and references

1 Y. H. Zhou, P. H. L and G. C. Wang, *J. Mol Catal. A: Chem.*, 2006, **258**, 203-215.
2 G. C. Wang, Y. H. Zhou, Y. Morikawa, J. Nakamura, Z. S. Cai and X. Z. Zhao, *J. Phys. Chem. B*, 2005, **109**, 12431-12442.
3 S. Sakong and A. Groß, *J. Catal.*, 2005, **231**, 420-429.
4 J. Greeley and M. Mavrikakis, *J. Catal.*, 2002, **208**, 291-300.
5 W. S. Sim, P. Gardner and D. A. King, *J. Phys. Chem.*, 1995, **99**, 16002-16010.
6 C. J. Zhang and P. Hu, *J. Chem. Phys.*, 2001, **115**, 7182-7186.
7 K. H. Lim, Z. X. Chen, K. M. Neyman and N. Rösch, *J. Phys. Chem. B*, 2006, **110**, 14890-14897.
8 R. Schennach, A. Eichler and K. D. Rendulic, *J. Phys. Chem. B*, 2003, **107**, 2552-2558.
9 Z. X. Chen, K. M. Neyman, K. H. Lim and N. Rösch, *Langmuir*, 2004, **20**, 8068-8077.
10 R. B. Jiang, W. Y. Guo, M. Li, D. L. Fu and H. H. Shan, *J. Phys. Chem. C*, 2009, **113**, 4188-4197.
11 S. K. Desai, M. Neurock and K. Kourtakis, *J. Phys. Chem. B*, 2002, **106**, 2559-2568.
12 J. Greeley and M. Mavrikakis, *J. Am. Chem. Soc.*, 2004, **126**, 3910-3919.
13 M. T. Koper, T. E. Shubina and R. A. van Santen, *J. Phys. Chem. B*, 2002, **106**, 686-692.
14 Y. Li and M. Bowker, *Catal. Today*, 1991, **10**, 421-424.
15 R. B. Jiang, W. Y. Guo, M. Li, H. Y. Zhu, L. M. Zhao, X. Q. Lu and H. H. Shan, *J. Mol. Catal. A: Chem.*, 2011, **344**, 99-110.
16 A. A. Deckert, J. L. Brand, C. H. Mak, B. G. Koehler and S. M. George, *J. Chem. Phys.*, 1987, **87**, 1936-1947.
17 R. B. Barros, A. R. Garcia and L. M. Ilharco, *J. Phys. Chem. B*, 2001, **105**, 11186-11193.
18 P. Gazdzicki, P. Uvdal and P. Jakob, *J. Chem. Phys.*, 2009, **130**, 224703.
19 P. Gazdzicki and P. Jakob, *J. Phys. Chem. C*, 2010, **114**, 2655-2663.
20 G. Q. Lu and A. Wieckowski, *Curr. Opin. Colloid Interface Sci.*, 2000, **5**, 95-100.
21 U. A. Paulus, U. Endruschat, G. J. Feldmeyer, T. J. Schmidt, H. Bönnemann and R. J. Behm, *J. Catal.*, 2000, **195**, 383-393.
22 E. Antolini, *Mater. Chem. and Phys.*, 2003, **78**, 563-573.
23 Q. Y. Lu, B. Yang, L. Zhuang and J. T. Lu, *J. Phys. Chem. B*, 2005, **109**, 1715-1722.
24 H. S. Liu, C. J. Song, L. Zhang, J. J. Zhang, H. J. Wang and D. P. Wilkinson, *J. Power Sources*, 2006, **155**, 95-110.
25 R. B. Barros, A. R. Garcia and L. M. Ilharco, *J. Phys. Chem. B*, 2004, **108**, 4831-4839.
26 R. B. Barros, A. R. Garcia and L. M. Ilharco, *Chem. Phys. Chem.*, 2005, **6**, 1299-1306.
27 R. Brito de Barros, A. R. Garcia and L. M. Ilharco, *Surf. Sci.*, 2003, **532–535**, 185-190.
28 J. S. Spendelow, J. D. Goodpaster, P. J. A. Kenis and A. Wieckowski, *J. Phys. Chem. B*, 2006, **110**, 9545-9555.
29 X. Q. Gong, P. Hu and R. Raval, *J. Chem. Phys.*, 2003, **119**, 6324-6334.
30 E. A. Batista, T. Iwasita and W. Vielstich, *J. Phys. Chem. B*, 2004, **108**, 14216-14222.

31 M. Yin, Y. J. Huang, L. Liang, J. H. Liao, C. P. Liu and W. Xing, *Chem. Commun.*, 2011, **47**, 8172-8174.
32 D. W. Yuan, X. G. Gong and R. Q. Wu, *J. Chem. Phys.*, 2008, **128**, 064706.
33 S. Park, Y. Xie and M. J. Weaver, *Langmuir*, 2002, **18**, 5792-5798.
34 B. Delley, *J. Phys. Chem.*, 1996, **100**, 6107-6110.
35 J. P. Perdew and Y. Wang, *Phys. Rev. B*, 1992, **45**, 13244-13249.
36 J. P. Perdew and W. Yue, *Phys. Rev. B*, 1986, **33**, 8800-8802.
37 B. Delley, *Phys. Rev. B*, 2002, **66**, 155125.
38 X. Q. Lu, Z. G. Deng, K. S. Chau, L. F. Li, Z. Q. Wen, W. Y. Guo and C. M. L. Wu, *ChemCatChem*, 2013, **5**, 1832-1841.
39 Z. G. Deng, X. Q. Lu, Z. Q. Wen, S. X. Wei, Y. J. Liu, D. L. Fu, L. M. Zhao and W. Y. Guo, *Phys. Chem. Chem. Phys.*, 2013, **15**, 16172-16182.
40 L. M. Zhao, S. P. Wang, Q. Y. Ding, W. B. Xu, P. P. Sang, Y. H. Chi, X. Q. Lu and W. Y. Guo, *J. Phys. Chem. C*, 2015, **119**, 20389-20400.
41 T. A. Halgren and W. N. Lipscomb, *Chem. Phys. Lett.*, 1977, **49**, 225-232.
42 X. Q. Lu, Z. G. Deng, S. X. Wei, Q. Y. Zhu, W. L. Wang, W. Y. Guo and C. M. L. Wu, *Catal. Sci. Technol.*, 2015, **5**, 3246-3258.
43 D. J. Chadi, *Phys. Rev. B*, 1977, **16**, 1746-1747.
44 D. R. Lide, ed., *Handb.Chem. Phys.*, CRC Press, Boca Raton, FL, 2000.
45 M. Mavrikakis and M. A. Barteau, *J. Mol. Catal. A: Chem.*, 1998, **131**, 135-147.
46 B. A. Sexton and A. E. Hughes, *Sur. Sci.*, 1984, **140**, 227-248.
47 J. Miragliotta, R. S. Polizzotti, P. Rabinowitz, S. D. Cameron and R. B. Hall, *Chem. Phys.*, 1990, **143**, 123-130.
48 M. N. D. S. Cordeiro, A. S. S. Pinto and J. A. N. F. Gomes, *Surf. Sci.*, 2007, **601**, 2473-2485.
49 R. Shekhar, M. A. Barteau, R. V. Plank and J. M. Vohs, *J. Phys. Chem. B*, 1997, **101**, 7939-7951.
50 M. A. Barteau, J. Q. Broughton and D. Menzel, *Surf. Sci.*, 1983, **133**, 443-452.
51 M. Y. Chou and J. R. Chelikowsky, *Phys. Rev. Lett.*, 1987, **59**, 1737-1740.
52 A. V. de Carvalho, M. C. Asensio and D. P. Woodruff, *Surf. Sci.*, 1992, **273**, 381-384.
53 X. K. Gu and W. X. Li, *J. Phys. Chem. C*, 2010, **114**, 21539-21547.
54 P. Ferrin and M. Mavrikakis, *J. Am. Chem. Soc.*, 2009, **131**, 14381-14389.
55 P. Ferrin, A. U. Nilekar, J. Greeley, M. Mavrikakis and J. Rossmeisl, *Surf. Sci.*, 2008, **602**, 3424-3431.
56 S. Lin, R. S. Johnson, G. K. Smith, D. Xie and H. Guo, *Phys. Chem. Chem. Phys.*, 2011, **13**, 9622-9631.
57 M. J. T. C. van der Niet, A. den Dunnen, L. B. F. Juurlink and M. T. M. Koper, *Angew. Chem. Int. Ed.*, 2010, **49**, 6572-6575.
58 J. K. Nørskov, J. Rossmeisl, A. Logadottir, L. Lindqvist, J. R. Kitchin, T. Bligaard and H. Jonsson, *J. Phys. Chem. B*, 2004, **108**, 17886-17892.
59 J. Rossmeisl, A. Logadottir and J. K. Nørskov, *Chem. Phys.*, 2005, **319**, 178-184.
60 G. S. Karlberg, J. Rossmeisl and J. K. Norskov, *Phys. Chem. Chem. Phys.*, 2007, **9**, 5158-5161.
61 *CRC Handb. Chem. Phys.*, CRC Press, New Yorkj, 1996.
62 P. Gazdzicki and P. Jakob, *J. Phys. Chem. C*, 2010, 114, 2655-2663.

GRAPHICAL ABSTRACT:

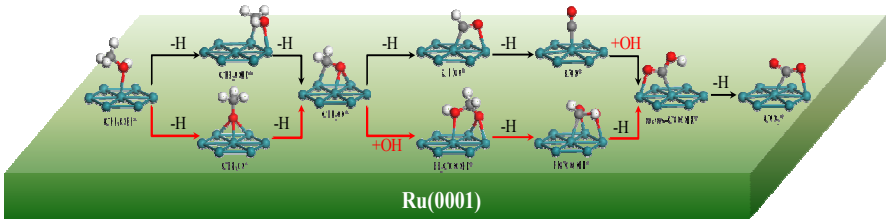

Competitive oxidation pathways of CH_3OH to CH_2O occur via $CH_3OH \rightarrow CH_3O \rightarrow CH_2O$ *vs.* $CH_3OH \rightarrow CH_2OH \rightarrow CH_2O$, further to COOH by virtue of OH group via $CH_2O \rightarrow CHO \rightarrow CO + OH \rightarrow COOH$ *vs.* $CH_2O + OH \rightarrow CH_2OOH \rightarrow CHOOH \rightarrow COOH$, and finally oxidation to CO_2 on Ru(0001).